RSC Advances

PAPER

View Article Online
View Journal | View Issue

Cite this: *RSC Adv.*, 2014, **4**, 52702

Design, synthesis and biological evaluation of (1,3-diphenyl-1*H*-pyrazol-4-yl) methyl benzoate derivatives as potential BRAF^{V600E} inhibitors

Ya-Juan Qin,†[a] Man Xing,†[a] Ya-Liang Zhang,[a] Jigar A. Makawana,[a] Ai-Qin Jiang*[b] and Hai-Liang Zhu*[a]

Received 15th August 2014
Accepted 15th October 2014

DOI: 10.1039/c4ra08708a

www.rsc.org/advances

A series of (1,3-diphenyl-1*H*-pyrazol-4-yl) methyl benzoate derivatives (**6a–10d**) were designed, synthesized and evaluated as BRAF^{V600E} inhibitors. Biological evaluation assays indicated that compound **10a** showed the most potent inhibitory activity against A375, WM266.4 and BRAF^{V600E} *in vitro* with IC_{50} values of 1.36 μM, 0.94 μM and 0.11 μM respectively compared with the positive compound vemurafenib. Furthermore, compound **10a** showed highly selective BRAF^{V600E} inhibitory activity *in vitro*. A docking simulation displayed that compound **10a** could tightly bind the crystal structure of BRAF^{V600E} at the active site. 3D-QSAR would provide a guideline to design and optimize more potent and positive BRAF^{V600E} inhibitors based on the (1,3-diphenyl-1*H*-pyrazol-4-yl) methyl benzoate derivatives skeleton.

1. Introduction

The MAPK signaling pathway consists of the Ras/Raf/MEK/ERK signal transduction cascade which is a vital mediator of a number of cellular fates including growth, proliferation, survival and differentiation in response to many different external stimuli such as growth factors, cytokines, and hormones. The MAPK pathway is also a common pathway that is activated at abnormally high levels in various human cancers. RAF kinases are vital players in the MAPK signal transduction pathway and are also important for regulating cell proliferation, survival and angiogenesis in a variety of cancer models. If this pathway is mutated and constantly switched on, the cell proliferation can have damaging effects, resulting in cancer.[1–3] This pathway is becoming an important point of current human cancer therapeutics and our group has been doing research on the pathway for many years, especially the RAF.

In mammalian cells there are three members of the RAF family, ARAF, BRAF and CRAF. The discovery of the most frequent V600E (>85%) BRAF mutations in 66% of melanoma, 45% of sporadic papillary thyroid cancers, 33% of KRAS mutated pancreatic cancers, and 15% of sporadic colorectal cancer have raised the expectation for targeted therapy. The V600E BRAF mutations show a 500-fold increase in catalytic activity, providing cancer cells with both proliferation and survival signals.[4–10]

In melanoma, BRAF^{V600E} stimulates proliferation and survival; inhibition of BRAF signaling with siRNA inhibits proliferation and induces apoptosis. These data validate BRAF as an important and exciting therapeutic target in human melanoma.[11,12] Lots of potent biochemical inhibitors of RAF were in clinical trials. Among them, the most studied BRAF inhibitor, Sorafenib (Bay 43-9006, Nexavar), was approved by the FDA in 2005 for the treatment of renal cell carcinoma and in 2007 for the treatment of hepatocellular carcinoma, and is still undergoing multiple clinical trials in other types of cancer.[6,13,14] It is probable because it also inhibits a number of other kinases (such as VEGFR, PDGFR).[15] So more potent and more selective inhibitors of BRAF^{V600E}, able to produce clinical results in melanoma, are needed.[16–20]

The general structure of BRAF kinase inhibitors (such as PLX4032 (ref. 21), RAF265, XL281 (ref. 22), L-779450, SB-590885 (ref. 23 and 24) and sorafenib) (Fig. 1) contains a H-bond donor, usually pyrazole, pyridine or imidazole heterocycle and a substituted aromatic group interacting with the hydrophobic pocket. In an attempt to find a better scaffold with optimal length for effective hydrogen bonding and hydrophobic interactions, we came up with (1,3-diphenyl-1*H*-pyrazol-4-yl) methyl benzoate derivatives. This series compounds were envisaged as having two purposes: the length of pyrazol bicycle was short for an effective hydrogen bonding with Glu_{500} and Asp_{593} (the sorafenib binding site).[18] In addition, the substituted benzoic acid skeleton can afford a hydrophobic complementarity interaction with secondary pocket of BRAF protein.

Many pyrazole derivatives were recently reported as potent BRAF^{V600E} inhibitors in our group.[25,26] In order to extend our research, herein we report the synthesis of a series of (1*H*-pyrazol-4-yl) methyl benzoate derivatives as BRAF^{V600E}

[a]*State Key Laboratory of Pharmaceutical Biotechnology, School of Life Science, Nanjing University, Nanjing 210093, P. R. China. E-mail: zhuhl@nju.edu.cn; Fax: +86-25-8359-2672; Tel: +86-25-8359-2572*

[b]*School of Medicine, Nanjing University, Nanjing, 210093, P. R. China*

† These two authors equally contributed to this paper.

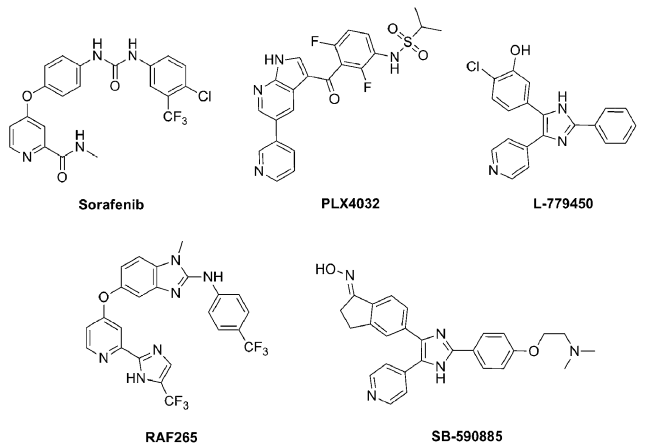

Fig. 1 Examples of chemical structures of $BRAF^{V600E}$ inhibitors.

inhibitors. Biological evaluation indicated that compound **10a** was found to be a potent and selective inhibitor of $BRAF^{V600E}$. Docking simulations were performed using the X-ray crystallographic structure of $BRAF^{V600E}$ in complex with an inhibitor to explore the binding modes of these compounds at the active site. In addition, based on the biological activity data, QSAR model was built to study the structure–activity relationship and guide the further study.

2. Results and discussion

2.1. Chemistry

The synthetic route of the (1*H*-pyrazol-4-yl) methyl benzoate derivatives (**6a–10d**) is outlined in Scheme 1. Synthesis of (1,3-diphenyl-1*H*-pyrazol-4-yl) methanol (**6–10**) was obtained from 1,3-diphenyl-1*H*-pyrazole-4-carbaldehyde using $NaBH_4$ as a reducing agent. (1,3-Diphenyl-1*H*-pyrazol-4-yl) methanol (**6–10**), benzoyl chloride and triethylamine were dissolved in dichloromethane and refluxed to give the desired compounds **6a–10d**. All synthesized compounds give satisfactory elementary analytical and spectroscopic data. ^1H NMR, ^{13}C NMR and ESI-MS spectra were consistent with the assigned structures.

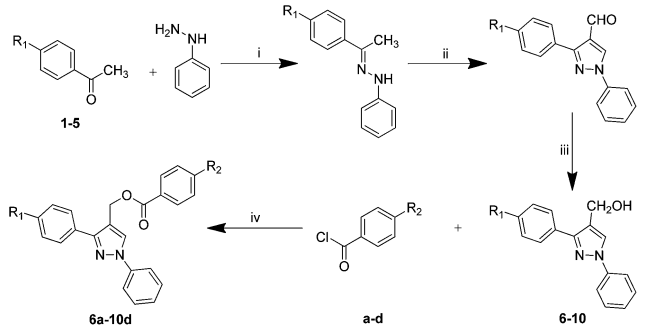

Scheme 1 General synthesis of (1,3-diphenyl-1*H*-pyrazol-4-yl) methyl benzoate derivatives (**6a–10d**). Reagents and conditions: (i) ethanol, 50–60 °C, 3 h; (ii) DMF, $POCl_3$, 50–60 °C, 5 h; (iii) $NaBH_4$,-ethanol, 0 °C; (iv) EDC, HOBt, CH_2Cl_2, refluxed, 8–10 h.

2.2. Crystal structure of compound 9c

Among all compounds, the crystal structure of compound **9c** was determined by X-ray diffraction analysis. The crystal data presented in Table 1 and Fig. 2 gives perspective views of compound **9c** with the atomic labeling system.

2.3. Pharmacology

2.3.1. Antiproliferative activities. Antiproliferative activity of synthesized compounds **6a–10d** was carried out against two cancer cell lines (A375 and WM266.4). The results were summarized in Table 2. (1,3-Diphenyl-1*H*-pyrazol-4-yl) methyl benzoate derivatives (**6a–10d**) showed remarkable anti-proliferative effects. Among them, compound **10a** displayed the most potent inhibitory activity against A375 and WM266.4 (IC_{50} = 1.36 μM, 0.94 μM respectively) as compared to the positive control vemurafenib (IC_{50} = 0.06 μM for WM266.4 and IC_{50} = 0.20 μM for A375 respectively).

2.3.2. BRAF inhibitory activity. The (1,3-diphenyl-1*H*-pyrazol-4-yl) methyl benzoate **6a–10d** were evaluated for their inhibitory for $BRAF^{V600E}$ using a solid-phase ELISA assay. **10c**, **10b** and **10a** showed strong inhibitory effect (IC_{50} = 1.15 μM, 0.63 μM and 0.11 μM, respectively). Compound **10a** displayed the most potent anti-BRAF activity (Table 2). This result indicated that the anti-proliferative effect was produced by direct connection of BRAF protein and the compounds.

Structure–activity relationships of synthesized derivatives indicate that compounds with *para*-electron-donating substituents (**10a**, **9a**) showed more potent activities than those with electron-withdrawing substituents (**7a**, **6a**) in A-ring. A comparison of the *para*-substituents on A-ring demonstrated that an electron-donating group (**10a**, **9a**) has slightly improved $BRAF^{V600E}$ inhibitory activity and the potency order is –OMe > –Me, whereas a Cl (**7a**) and F (**6a**) group substituent has minimal

Table 1 Crystallographical and experimental data for compound **9c**

Compounds	**9c**
Empirical formula	$C_{24}H_{20}N_2O_2$
Formula weight	368.42
Crystal system	Triclinic
Space group	$P\bar{1}$
a (Å)	8.2744(9)
b (Å)	9.9739(12)
c (Å)	12.4229(13)
a (°)	81.884(4)
b (°)	78.048(3)
c (°)	77.788(4)
V (Å)	975.22(19)
Z	2
D_{calcd}/g cm^{-3}	1.255
H range (°)	1.68–25.20
F(000)	388
Reflections collected/unique	9365/3473
Data/restraints/parameters	3473/0/254
Absorption coefficient (mm^{-1})	0.081
R_1; wR_2 [$I > 2\sigma(I)$]	0.0497/0.1222
R_1; wR_2 (all data)	0.0942/0.1433
GOF	1.024

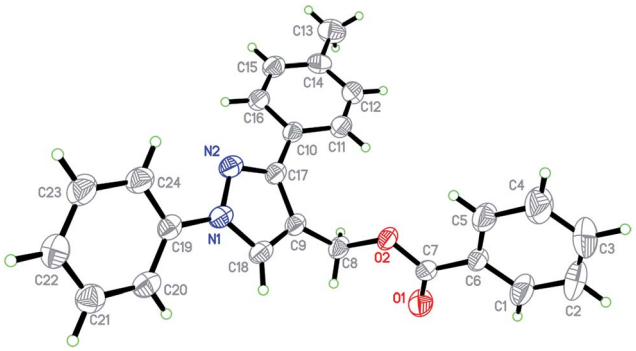

Fig. 2 Crystal structure diagram of compound **9c**. H atoms are shown as small spheres of arbitrary radii.

effects compared with **8a**. In the case of constant A ring substituents, change of substituents on B ring could also affect the activities of compounds. Among compounds **10a–10d**, compounds with *para* electron-withdrawing substituted (**10a**, **10b**) showed stronger anticancer activities and the strength order was different from A ring: –F > –Cl > –H > –OMe, followed that **10d** showed the lowest activity. Among all the compounds, **10a** with *para*-OMe and F group in the A and B ring respectively, leads to a noteworthy best activity. The following molecular docking of all the synthesized compounds also showed this result and indicated that these compounds were potential $BRAF^{V600E}$ inhibitory agents.

2.3.3. Kinase selectivity. To evaluate potential inhibition of other kinases beyond $BRAF^{V600E}$, we tested the compound **10a**

Table 2 Inhibition (IC_{50}) of A375, WM266.4 and $BRAF^{V600E}$ by compounds (1,3-diphenyl-1*H*-pyrazol-4-yl) methyl benzoate derivatives (**6a–10d**)

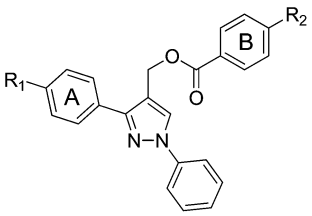

Compounds	R_1	R_2	$IC_{50} \pm SD$ (μM) A375	WM266.4	$BRAF^{V600E}$
6a	F	F	7.72 ± 0.59	5.12 ± 0.45	3.82 ± 0.91
6b	F	Cl	8.63 ± 0.85	6.01 ± 0.67	4.01 ± 0.71
6c	F	H	8.81 ± 1.01	7.23 ± 0.77	12.0 ± 1.12
6d	F	OMe	11.71 ± 2.25	13.44 ± 1.12	10.9 ± 1.13
7a	Cl	F	7.08 ± 0.91	5.23 ± 0.23	3.86 ± 0.38
7b	Cl	Cl	8.64 ± 1.15	6.33 ± 1.23	3.56 ± 0.32
7c	Cl	H	9.04 ± 1.37	8.34 ± 1.04	6.06 ± 0.65
7d	Cl	OMe	16.91 ± 1.57	14.33 ± 1.22	8.02 ± 0.88
8a	H	F	5.83 ± 0.89	5.33 ± 0.25	3.79 ± 0.07
8b	H	Cl	7.92 ± 0.91	5.23 ± 0.73	4.12 ± 0.38
8c	H	H	7.05 ± 1.35	6.33 ± 0.45	5.01 ± 0.59
8d	H	OMe	9.13 ± 1.63	8.83 ± 0.98	5.91 ± 0.71
9a	Me	F	5.78 ± 0.51	3.44 ± 0.17	1.41 ± 0.04
9b	Me	Cl	8.88 ± 0.66	8.33 ± 1.21	6.56 ± 0.05
9c	Me	H	8.09 ± 0.73	6.44 ± 0.77	5.68 ± 0.06
9d	Me	OMe	9.65 ± 0.91	8.33 ± 1.02	5.78 ± 0.07
10a	OMe	F	1.36 ± 0.07	0.94 ± 0.05	0.11 ± 0.01
10b	OMe	H	2.09 ± 0.43	1.33 ± 0.78	0.63 ± 0.22
10c	OMe	Cl	2.78 ± 0.37	2.45 ± 0.32	1.15 ± 0.01
10d	OMe	OMe	8.76 ± 0.49	7.34 ± 0.89	4.38 ± 0.41
Vemurafenib			0.20 ± 0.02	0.06 ± 0.007	0.03 ± 0.006

Table 3 Kinase selectivity of compound **10a**

Kinase	IC_{50} (μM)	Kinase	IC_{50} (μM)
p38α	N.i.[a]	CDK1/CycB	11
$BRAF^{V600E}$	0.11	CDK2/CycA	18
Aurora-A	13	VEGFR2	N.i.
Aurora-B	15	PDGFRα	N.i
MEK1	N.i.	cSrc	N.i.

[a] N.i.: no inhibition, IC_{50} > 20 μM.

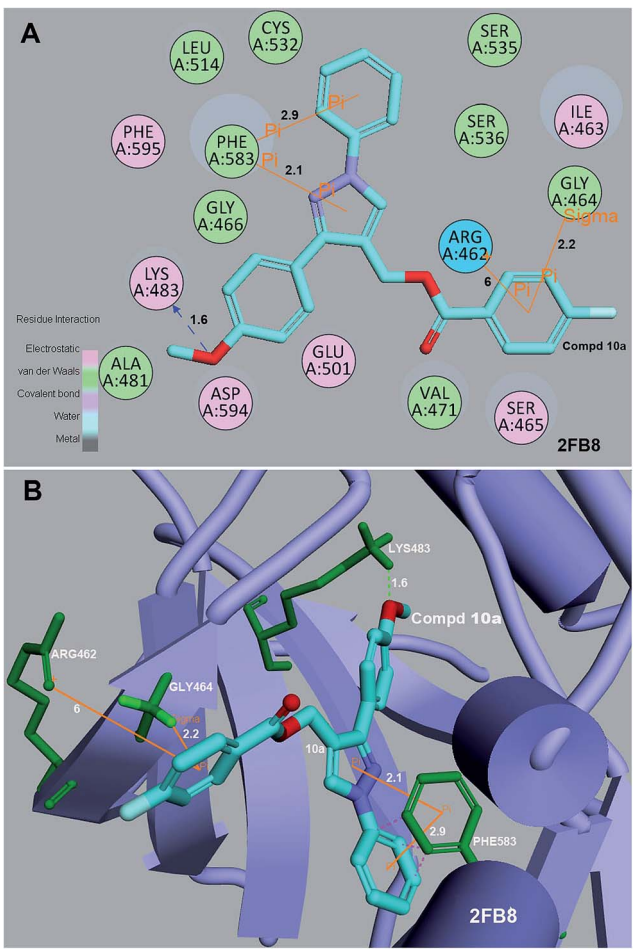

Fig. 3 The binding mode between the active conformation of compound **10a** and the target protein $BRAF^{V600E}$ (PDB code: 2FB8) provided by the CDOCKER protocol (Discovery Studio 3.5, Accelrys, Co. Ltd). We employed 2D diagram (A), 3D interaction map (B) to display the interaction between **10a** and the targeted protein. In the binding model, compound **10a** is nicely bound to 2FB8 *via* one hydrogen bond, three π–π interaction and one π–sigma interaction.

in a selectivity study towards a panel of 10 different kinases, and the results were reported in Table 3. Four kinases (p38α, MEK1, VEGFR2, PDGFRα, and cSrc) were inhibited by compound **10a** with IC_{50} over 20 μM. Selectivity for $BRAF^{V600E}$ was also more than 1000-fold as well as other protein kinases.

2.4. Molecular docking study

To gain better understanding on the potency of the studied compounds and guide further SAR studies, we proceeded to examine the interaction of compounds **6a–10d** with $BRAF^{V600E}$ (PDB code: 2FB8). All docking runs were applied LigandFit Dock protocol of Discovery Studio 3.5. The binding modes of compound **10a** and BRAF were depicted in Fig. 3 and 4. Visual inspection of the pose of compound **10a** into $BRAF^{V600E}$ binding site revealed that compound **10a** was tightly embedded into the active binding pocket (Fig. 4). In the binding mode, compound **10a** is potently bound to the active binding site of $BRAF^{V600E}$ *via* one hydrogen bond, three π–π interactions and one π–sigma interaction. The oxygen atoms of the A ring formed one hydrogen bond with the amino hydrogen of Lys A: 483 (bond length: Lys A: 483 N–H···O = 1.6 Å); contribute to the hydrogen bonding interaction together, being a probable explanation for its nice activity. On the other hand, the A ring formed one π–π interaction and one π–sigma interaction with ARG A: 462 (bond length: 6.0 Å) and ARG A: 464 (bond length: 2.0 Å) respectively. The binding model also showed that there were three π–π interactions between phenyl pyrazole ring of compound **10a** and PHE A: 583. Overall, these results of the molecular docking study showed that (1,3-diphenyl-1*H*-pyrazol-4-yl) methyl benzoate derivatives could act synergistically to interact with the active binding site of $BRAF^{V600E}$, suggested that compound **10a** is a potential inhibitor of $BRAF^{V600E}$.

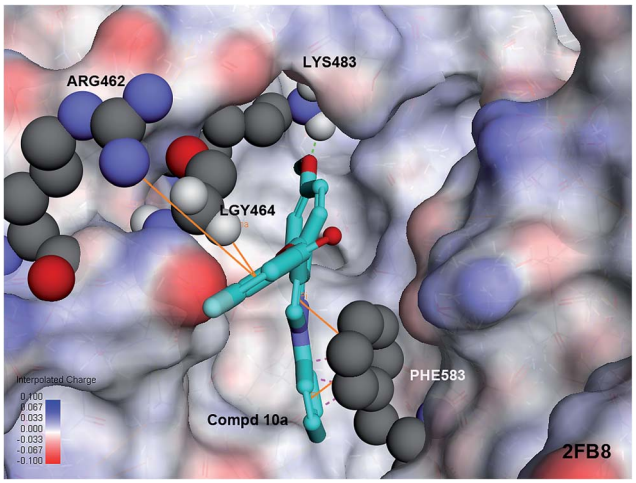

Fig. 4 The surface model structure to display the interaction between **10a** and the $BRAF^{V600E}$.

2.5. 3D-QSAR

In order to obtain a systematic SAR profile on (1,3-diphenyl-1*H*-pyrazol-4-yl) methyl benzoate derivatives as $BRAF^{V600E}$ inhibitors as well as to explore the more potent and selective $BRAF^{V600E}$ inhibitors, 3D-QSAR model was built using the corresponding pIC_{50} values which were converted from the obtained IC_{50} (μM) values of $BRAF^{V600E}$ kinase inhibition and performed by built-in QSAR software of DS 3.5 (Discovery Studio 3.5, Accelrys, Co. Ltd). The way of this transformation was derived from an online calculator developed from an indian medicinal chemistry lab (http://www.sanjeevslab.org/tools-IC50.html). The training and test set was divided by the random diverse molecules method of DS 3.5, in which the training set accounts for 80% and the test set was set to 20%. The training set was composed of 16 agents and the relative test set comprised 4 agents. In default situation, the alignment

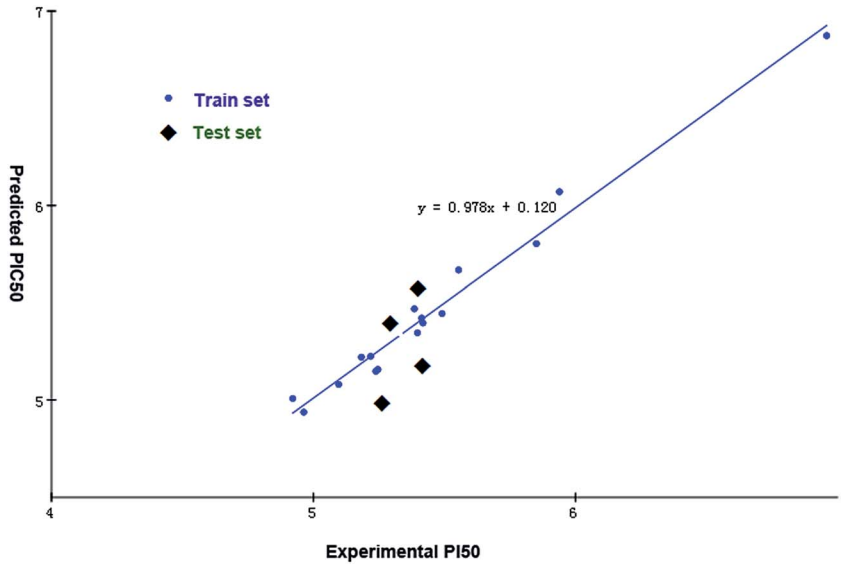

Fig. 5 The predicted *versus* experimental pIC_{50} values for the inhibition of $BRAF^{V600E}$ (PDB: 2FB8).

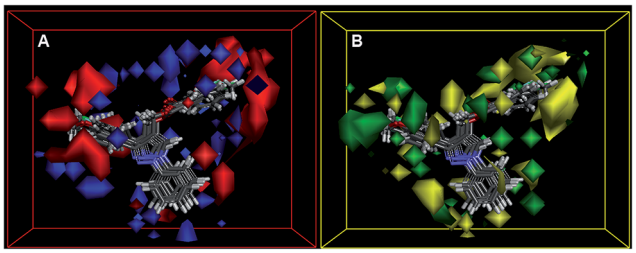

Fig. 6 (A) Isosurface of the 3D-QSAR model coefficients on electrostatic potential grids. The blue triangle mesh represents positive electrostatic potential and the red area represents negative electrostatic potential. (B) Isosurface of the 3D-QSAR model coefficients on van der Waals grids. The green triangle mesh representation indicates positive coefficients; the yellow triangle mesh indicates negative coefficients.

conformation of each molecule was the one that possessed the lowest CDOCKER_INTERACTION_ENERGY among the twenty docked poses. The 3D-QSAR model generated from DS 3.5, defined the critical regions (steric or electrostatic) affecting the binding affinity. It was a PLS model built on 400 independent variables (conventional $r^2 = 0.978$). Moreover, their graphical relationship had been illustrated in Fig. 5, in which the plot of the observed IC_{50} *versus* the predicted values showed that this model could be used in prediction of activity for (1,3-diphenyl-1*H*-pyrazol-4-yl) methyl benzoate derivatives as $BRAF^{V600E}$ inhibitors.

A contour plot of the electrostatic field region favorable (in blue) and unfavorable (red) for anticancer activity based on $BRAF^{V600E}$ protein target were shown in Fig. 6A while the energy grids corresponding to the favorable (in green) or unfavorable (yellow) steric effects for the $BRAF^{V600E}$ affinity were shown in Fig. 6B. It was widely acceptable that a better inhibitor based on the 3D-QSAR model should have strong van der Waals attraction in the green areas and a polar group in the blue electrostatic potential areas (which were dominant close to the skeleton). Thus, this promising model would provide a guideline to design and optimize more effective $BRAF^{V600E}$ inhibitors based on the (1,3-diphenyl-1*H*-pyrazol-4-yl) methyl benzoate derivatives skeleton and provide us the direction of further modification.

3. Conclusion

In our present work, a series of anticancer inhibitors (1,3-diphenyl-1*H*-pyrazol-4-yl) methyl benzoate derivatives (**6a–10d**) has been synthesized and biologically evaluated. These compounds exhibited $BRAF^{V600E}$ inhibitory activities and antiproliferative activities against A375 and WM266.4 cell lines. Among them, compound **10a** demonstrated the most potent activity which inhibited the growth of A375 and WM266.4 cancer cell lines with IC_{50} values of 1.36 and 0.94 μM respectively, and inhibited $BRAF^{V600E}$ inhibitory activity with an IC_{50} of 0.11 μM. Furthermore, compound **10a** showed highly selective potent $BRAF^{V600E}$ inhibitory activity *in vitro*. Molecular docking showed that compound **10a** bound to the binding site by one hydrogen bond, three π–π bonds which might play a crucial role in its $BRAF^{V600E}$ inhibition and antiproliferative activity. This study might be helpful for the design and synthesis of $BRAF^{V600E}$ and tumor growth inhibitors with stronger activities. QSAR model was built to provide a reliable tool for reasonable design of novel $BRAF^{V600E}$ inhibitors in future.

4. Experimental protocols

4.1. Materials and measurements

All chemicals and reagents used in current study were of analytical grade. All the ^1H NMR and ^{13}C NMR spectra were recorded on a Bruker DPX300 model Spectrometer in DMSO-d_6 at 25 °C with TMS and chemical shifts were reported in ppm (δ). ESI-MS spectra were recorded on a Mariner System 5304 Mass spectrometer. Elemental analyses were performed on a CHN–O-Rapid instrument. Elemental analyses were performed on a CHN–O-Rapid instrument. All the compounds gave satisfactory chemical analyses (±0.4%). TLC was performed on the glass-backed silica gel sheets (Silica Gel 60 GF254) and visualized in UV light (254 nm). Column chromatography was performed using silica gel (200–300 mesh) eluting with ethyl acetate and petroleum ether.

4.2. Synthesis

4.2.1. General synthetic procedure of (1,3-diphenyl-1*H*-pyrazole-4-carbaldehyde) (6–10). The starting material 1,3-diphenyl-1*H*-pyrazole-4-carbaldehyde (**6–10**) was synthesized based on a literature method.[27–29] 1-Phenyl-2-(1-phenylethylidene) hydrazine (**1–5**) (3.6 g, 0.015 mol) was added to a cold solution of DMF (25 ml), then $POCl_3$ (5 ml) was added and the resulting mixture was stirred at 50–60 °C for 6 h. The mixture was poured into ice-cold water. A saturated solution of sodium hydroxide was added to neutralize the mixture, and then the solid precipitate was filtered, washed with water, dried and recrystallized from ethanol.

4.2.2. General synthetic procedure of (1,3-diphenyl-1*H*-pyrazol-4-yl) methanol. A solution of 0.76 g (0.02 mol) of sodium tetrahydridoborate in ethanol (100 ml) was added with stirring to a solution of 0.02 mol of 1,3-diphenyl-1*H*-pyrazole-4-carbaldehyde (**6–10**) in ethanol (60 ml). The mixture was stirred for 1 h, 200 ml of water was added, and the mixture was left to stand for 12 h at 0 °C. The precipitate was filtered off, washed with water, dried, and recrystallized from ethanol.

4.2.3. General synthetic procedure of (1,3-diphenyl-1*H*-pyrazol-4-yl) methyl benzoate (6a–10d). Compounds **6a–10d** were synthesized by coupling (1,3-diphenyl-1*H*-pyrazol-4-yl) methanol with substituted benzoic acid, using 1-ethyl-3-(3-dimethylaminopropyl) carbodiimidehydrochloride and *N*-hydroxybenzotriazole (HOBt) as condensing agent. The mixture was refluxed in anhydrous CH_2Cl_2 for 8–10 h. The products were extracted with ethyl acetate. The extract was washed successively with 10% HCl, saturated $NaHCO_3$ and water, dried over anhydrous Na_2SO_4, filtered and evaporated. The residue was purified by column chromatography using petroleum ether and ethyl acetate (3 : 1).

4.3. Spectral properties of (1,3-diphenyl-1*H*-pyrazol-4-yl) methyl benzoate derivatives

4.3.1. (3-(4-Fluorophenyl)-1-phenyl-1-pyrazol-4-yl) methyl 4-fluorobenzoate (6a). Light yellow powder, yield 79%, mp: 151–154 °C; ^{1}H NMR (300 MHz, $CDCl_3$) δ ppm: 5.39 (s, 2H); 7.10 (t, J = 6.03 Hz, 2H); 7.16 (t, J = 4.98 Hz, 2H); 7.31 (d, J = 4.20 Hz, 1H); 7.46 (t, J = 4.57 HZ, 2H); 7.74 (d, J = 4.86 HZ, 2H); 7.81(t, J = 3.93 HZ, 2H); 8.05 (t, J = 4.13 HZ, 2H); 8.14 (s, 1H). ESI-MS: 391.38 ($C_{23}H_{17}F_2N_2O_2$ $[M + H]^+$). Anal. calcd for $C_{23}H_{17}F_2N_2O_2$: C, 70.76; H, 4.13; F, 9.73; N, 7.18; O, 8.20%. Found: C, 70.75; H, 4.14; F, 9.72; N, 7.19; O, 8.20%.

4.3.2. (3-(4-Fluorophenyl)-1-phenyl-1*H*-pyrazol-4-yl) methyl 4-chlorobenzoate (6b). White powder, yield 81%, mp: 180–182 °C; ^{1}H NMR (300 MHz, $CDCl_3$) δ ppm: 5.40 (s, 2H) 7.16 (t, J = 8.70 Hz, 2H); 7.31 (t, J = 7.41 Hz, 1H); 7.40–7.49 (m, 4H); 7.73–7.83 (m, 4H); 7.97 (t, J = 4.38 Hz, 2H); 8.16 (s, 1H). ESI-MS: 407.84 ($C_{23}H_{17}ClFN_2O_2$ $[M + H]^+$). Anal. calcd for $C_{23}H_{17}ClFN_2O_2$: C, 67.90; H, 3.96; Cl, 8.71; F, 4.67; N, 6.89; O, 7.87%. Found: C, 67.91; H, 3.95; Cl, 8.70; F, 4.68; N, 6.88; O, 7.88%.

4.3.3. (3-(4-Fluorophenyl)-1-phenyl-1*H*-pyrazol-4-yl) methyl benzoate (6c). White powder, yield 80%, mp: 131–133 °C; ^{1}H NMR (300 MHz, $CDCl_3$) δ ppm: 5.40 (s, 2H); 7.17 (t, J = 8.68 Hz, 2H); 7.30 (t, J = 7.32 Hz, 1H); 7.42–7.49 (m, 4H); 7.57 (t, J = 7.41 Hz, 1H); 7.75 (d, J = 8.07 Hz, 2H); 7.81–7.85 (m, 2H); 8.04 (t, J = 4.38 Hz, 2H); 8.16 (s, 1H). ^{13}C NMR (100 MHz, $CDCl_3$) δ ppm: 166.52, 164.18, 161.72, 151.74, 139.75, 133.24, 130.06, 129.82, 129.78, 129.70, 129.67, 129.52, 128.85, 128.81, 128.53, 126.81, 119.19, 115.88, 115.66, 115.57, 57.68. ESI-MS: 373.39 ($C_{23}H_{18}FN_2O_2$ $[M + H]^+$). Anal. calcd for $C_{23}H_{18}FN_2O_2$: C, 74.18; H, 4.60; F, 5.10; N, 7.52; O, 8.59%. Found: C, 74.17; H, 4.61; F, 5.11; N, 7.52; O, 8.59%.

4.3.4. (3-(4-Fluorophenyl)-1-phenyl-1*H*-pyrazol-4-yl) methyl 4-methoxybenzoate (6d). White powder, yield 81%, mp: 152–153 °C; ^{1}H NMR (300 MHz, $CDCl_3$) δ ppm: 3.85 (s, 3H); 5.37 (s, 2H); 6.91 (d, J = 5.31 Hz, 2H); 7.15 (t, J = 5.17 Hz, 2H); 7.30 (t, J = 4.33 Hz, 1H); 7.46 (t, J = 4.66 Hz, 2H); 7.75 (d, J = 4.83 Hz, 2H); 7.82 (t, J = 4.22 Hz, 2H); 7.99 (d, J = 5.31 Hz, 2H); 8.14 (s, 1H). ^{13}C NMR (100 MHz, $CDCl_3$) δ ppm: 166.25, 164.15, 163.56, 161.70, 151.68, 139.77, 131.72, 129.77, 129.69, 129.50, 128.90, 128.87, 126.76, 122.42, 119.16, 115.85, 115.79, 115.63, 113.77, 57.38, 55.50. ESI-MS: 403.42 ($C_{24}H_{20}FN_2O_3$ $[M + H]^+$). Anal. calcd for $C_{24}H_{20}FN_2O_3$: C, 71.63; H, 4.76; F, 4.72; N, 6.96; O, 11.93%. Found: C, 71.63; H, 4.77; F, 4.71; N, 6.97; O, 11.92%.

4.3.5. (3-(4-Chlorophenyl)-1-phenyl-1*H*-pyrazol-4-yl) methyl 4-fluorobenzoate (7a). Light yellow powder, yield 85%, mp: 136–138 °C; ^{1}H NMR (300 MHz, $CDCl_3$) δ ppm: 5.40 (s, 2H); 7.11 (t, J = 5.16 Hz, 2H); 7.31 (t, J = 4.49 Hz, 1H); 7.44–7.48 (m, 4H); 7.74–7.79 (m, 4H); 8.03–8.06 (m, 2H); 8.15 (s, 1H). ESI-MS: 408.84 ($C_{23}H_{17}ClFN_2O_2$ $[M + H]^+$). Anal. calcd for $C_{23}H_{17}ClFN_2O_2$: C, 67.90; H, 3.96; Cl, 8.71; F, 4.67; N, 6.89; O, 7.87%. Found: C, 67.91; H, 3.95; Cl, 8.70; F, 4.68; N, 6.88; O, 7.88%.

4.3.6. (3-(4-Chlorophenyl)-1-phenyl-1*H*-pyrazol-4-yl) methyl 4-chlorobenzoate (7b). White powder, yield 77%, mp: 175–177 °C; ^{1}H NMR (300 MHz, $CDCl_3$) δ ppm: 5.40 (s, 2H); 7.31 (t, J = 7.41 Hz, 1H); 7.40–7.49 (m, 6H); 7.73–7.79 (m, 4H); 7.95–7.98 (m, 2H); 8.15 (s, 1H). ESI-MS: 424.29 ($C_{23}H_{17}Cl_2N_2O_2$ $[M + H]^+$). Anal. calcd for $C_{23}H_{17}Cl_2N_2O_2$: C, 65.26; H, 3.81; Cl, 16.75; N, 6.62; O, 7.56%. Found: C, 65.25; H, 3.80; Cl, 16.74; N, 6.62; O, 7.59%.

4.3.7. (3-(4-Chlorophenyl)-1-phenyl-1*H*-pyrazol-4-yl) methyl benzoate (7c). White powder, yield 76%, mp: 147–148 °C; ^{1}H NMR (300 MHz, $CDCl_3$) δ ppm: 7.31–7.33 (m, 1H); 7.41–7.49 (m, 6H); 7.54–7.60 (m, 1H); 7.72–7.77 (m, 2H); 7.78–7.83 (m, 2H); 8.03–8.06 (m, 2H); 8.16 (s, 1H). ESI-MS: 389.85 ($C_{23}H_{18}ClN_2O_2$ $[M + H]^+$). Anal. calcd for $C_{23}H_{18}ClN_2O_2$: C, 71.04; H, 4.41; Cl, 9.12; N, 7.20; O, 8.23%. Found: C, 71.04; H, 4.42; Cl, 9.11; N, 7.21; O, 8.22%.

4.3.8. (3-(4-Chlorophenyl)-1-phenyl-1*H*-pyrazol-4-yl) methyl 4-methoxybenzoate (7d). Light yellow powder, yield 81%, mp: 150–152 °C; ^{1}H NMR (300 MHz, $CDCl_3$) δ ppm: 3.90 (s, 3H); 5.37 (s, 2H); 6.91 (d, J = 5.22 Hz, 2H); 7.30 (t, J = 4.44 Hz, 1H); 7.43–7.47 (m, 4H); 7.74 (d, J = 4.77 Hz, 2H); 7.80 (d, J = 5.04 Hz, 2H); 7.99 (d, J = 5.22 Hz, 2H); 8.14 (s, 1H). ESI-MS: 419.87 ($C_{24}H_{20}ClN_2O_3$ $[M + H]^+$). Anal. calcd for $C_{24}H_{20}ClN_2O_3$: C, 68.82; H, 4.57; Cl, 8.46; N, 6.69; O, 11.46%. Found: C, 68.81; H, 4.58; Cl, 8.45; N, 6.68; O, 11.48%.

4.3.9. (1,3-Diphenyl-1*H*-pyrazol-4-yl) methyl 4-fluorobenzoate (8a). Light yellow powder, yield 83%, mp: 94–95 °C; ^{1}H NMR (300 MHz, $CDCl_3$) δ ppm: 5.42 (s, 2H); 7.10 (t, J = 5.04 Hz, 2H); 7.30 (t, J = 4.39 Hz, 1H); 7.40 (t, J = 4.39 Hz, 1H); 7.44–7.48 (m, 4H); 7.76 (d, J = 4.86 Hz, 2H); 7.83 (d, J = 4.68 Hz, 2H); 8.06 (t, J = 3.93 Hz, 2H); 8.15 (s, 1H). ^{13}C NMR (100 MHz, $CDCl_3$) δ ppm: 167.14, 165.62, 164.62, 152.61, 139.81, 132.63, 132.30, 132.20, 129.73, 129.50, 128.79, 128.38, 127.98, 126.77, 126.40, 126.37, 119.21, 115.77, 115.61, 115.56, 57.92. ESI-MS: 373.39 ($C_{23}H_{18}FN_2O_2$ $[M + H]^+$). Anal. calcd for $C_{23}H_{18}FN_2O_2$: C, 74.18; H, 4.60; F, 5.10; N, 7.52; O, 8.59%. Found: C, 74.17; H, 4.61; F, 5.11; N, 7.53; O, 8.58%.

4.3.10. (1,3-Diphenyl-1*H*-pyrazol-4-yl) methyl 4-chlorobenzoate (8b). Light yellow powder, yield 79%, mp: 125–126 °C; ^{1}H NMR (300 MHz, $CDCl_3$) δ ppm: 5.43 (s, 2H); 7.30 (t, J = 8.68 Hz, 1H); 7.39–7.50 (m, 7H); 7.76 (d, J = 7.50 Hz, 2H); 7.83 (t, J = 4.20 Hz, 2H); 7.96–7.99 (m, 2H); 8.15 (s, 1H). ESI-MS: 389.85 ($C_{23}H_{18}ClN_2O_2$ $[M + H]^+$). Anal. calcd for $C_{23}H_{18}ClN_2O_2$: C, 71.04; H, 4.41; Cl, 9.12; N, 7.20; O, 8.23%. Found: C, 71.03; H, 4.42; Cl, 9.11; N, 7.21; O, 8.23%.

4.3.11. (1,3-Diphenyl-1*H*-pyrazol-4-yl) methyl benzoate (8c). White powder, yield 80%, mp: 75–77 °C; ^{1}H NMR (300 MHz, $CDCl_3$) δ ppm: 5.44 (s, 2H); 7.30 (t, J = 7.41 Hz, 1H); 7.40–7.50 (m, 7H); 7.56 (t, J = 7.41 Hz, 1H); 7.77 (d, J = 7.50 Hz, 2H); 7.86 (d, J = 7.14 Hz, 2H); 8.06 (t, J = 4.38 Hz, 2H); 8.17 (s, 1H). ESI-MS: 355.40 ($C_{23}H_{19}N_2O_2$ $[M + H]^+$). Anal. calcd for $C_{23}H_{19}N_2O_2$: C, 77.95; H, 5.12; N, 7.90; O, 9.03%. Found: C, 77.94; H, 5.11; N, 7.91; O, 9.04%.

4.3.12. (1,3-Diphenyl-1*H*-pyrazol-4-yl) methyl 4-methoxybenzoate (8d). Light yellow powder, yield 76%, mp: 91–93 °C; ^{1}H NMR (300 MHz, $CDCl_3$) δ ppm: 3.87 (s, 3H); 5.37 (s, 2H); 6.91 (d, J = 5.21 Hz, 2H); 7.15 (t, J = 5.19 Hz, 2H); 7.30 (t, J = 7.41 Hz, 1H) 7.40–7.50 (m, 2H); 7.46 (t, J = 6.41 Hz, 1H); 7.76 (d, J = 4.50 Hz, 2H); 7.84 (d, J = 7.02 Hz, 2H); 8.05 (t, J = 4.02 Hz, 2H); 8.17 (s, 1H). ESI-MS: 385.15 ($C_{24}H_{20}N_2O_3$ $[M + H]^+$). Anal. calcd for $C_{24}H_{20}N_2O_3$: C, 74.98; H, 5.24; N, 7.29; O, 12.49%. Found: C, 74.96; H, 5.22; N, 7.31; O, 12.51%.

4.3.13. (1-Phenyl-3-(*p*-tolyl)-1*H*-pyrazol-4-yl) methyl 4-fluorobenzoate (9a). Light yellow powder, yield 80%, mp: 117–119 °C; ^{1}H NMR (300 MHz, $CDCl_3$) δ ppm: 2.41 (s, 3H); 5.41 (s, 2H); 7.10 (t, J = 5.08 Hz, 2H); 7.29 (t, J = 4.71 Hz, 3H); 7.45 (t, J = 4.68 Hz, 2H); 7.71–7.76 (m, 4H); 8.04–8.07 (m, 2H); 8.14 (s, 1H). ESI-MS: 387.42 ($C_{24}H_{20}FN_2O_2$ $[M + H]^+$). Anal. calcd for $C_{24}H_{20}FN_2O_2$: C, 74.60; H, 4.96; F, 4.92; N, 7.25; O, 8.28%. Found: C, 74.61; H, 4.95; F, 4.93; N, 7.24; O, 8.28%.

4.3.14. (1-Phenyl-3-(*p*-tolyl)-1*H*-pyrazol-4-yl) methyl 4-chlorobenzoate (9b). White powder, yield 74%, mp: 139–140 °C; ^{1}H NMR (300 MHz, $CDCl_3$) δ ppm: 2.41 (s, 3H); 5.42 (s, 2H); 7.22–7.32 (m, 3H); 7.39–7.48 (m, 4H); 7.71–7.77 (m, 4H); 7.98 (d, J = 8.58 Hz, 2H); 8.14 (s, 1H). ESI-MS: 403.87 ($C_{24}H_{20}ClN_2O_2$ $[M + H]^+$). Anal. calcd for $C_{24}H_{20}ClN_2O_2$: C, 71.55; H, 4.75; Cl, 8.80; N, 6.95; O, 7.94%. Found: C, 71.56; H, 4.74; Cl, 8.81; N, 6.94; O, 7.95%.

4.3.15. (1-Phenyl-3-(*p*-tolyl)-1*H*-pyrazol-4-yl) methyl benzoate (9c). Light yellow powder, yield 77%, mp: 133–136 °C; ^{1}H NMR (300 MHz, $CDCl_3$) δ ppm: 2.35 (s, 3H); 5.42 (s, 2H); 7.30–7.36 (m, 3H); 7.50–7.55 (m, 4H); 7.64–7.72 (m, 3H); 7.90–7.97 (m, 5H). ESI-MS: 370.43 ($C_{24}H_{20}N_2O_2$ $[M + H]^+$). Anal. calcd for $C_{24}H_{20}N_2O_2$: C, 78.24; H, 5.47; N, 7.60; O, 8.69%. Found: C, 78.23; H, 5.48; N,7.59; O, 8.70%.

4.3.16. (1-Phenyl-3-(*p*-tolyl)-1*H*-pyrazol-4-yl) methyl 4-methoxybenzoate (9d). Light yellow powder, yield 82%, mp: 99–100 °C; ^{1}H NMR (300 MHz, $CDCl_3$) δ ppm: 2.41 (s, 3H); 3.86 (s, 3H); 5.40 (s, 2H); 6.91 (d, J = 5.13 Hz, 2H); 7.29 (t, J = 4.21 Hz, 4H); 7.45 (t, J = 4.53 Hz, 2H); 7.75 (t, J = 4.62 Hz, 4H); 8.01 (d, J = 5.04 Hz, 2H); 8.14 (s, 1H). ^{13}C NMR (100 MHz, $CDCl_3$) δ ppm: 166.32, 163.49, 152.63, 139.90, 138.13, 131.74, 129.83, 129.57, 129.45, 127.86, 126.58, 122.58, 119.16, 115.83, 113.71, 57.57, 55.49, 21.38. ESI-MS: 399.45 ($C_{25}H_{23}N_2O_3$ $[M + H]^+$). Anal. calcd for $C_{25}H_{23}N_2O_3$: C, 75.36; H, 5.57; N, 7.03; O, 12.05%. Found: C, 75.35; H, 5.56; N, 7.04; O, 12.05%.

4.3.17. (3-(4-Methoxyphenyl)-1-phenyl-1*H*-pyrazol-4-yl) methyl 4-fluorobenzoate (10a). White powder, yield 75%, mp: 104–107 °C; ^{1}H NMR (300 MHz, $CDCl_3$) δ ppm: 3.80 (s, 3H); 5.40 (s, 2H); 7.03 (d, J = 5.12 Hz, 2H); 7.35 (t, J = 4.24 Hz, 1H); 7.45 (d, J = 4.13 Hz, 2H); 7.65 (t, J = 4.75 Hz, 2H); 7.74–7.77 (m, 4H); 8.03 (d, J = 4.31 Hz, 2H); 8.13 (s, 1H). ESI-MS: 403.14 ($C_{24}H_{19}FN_2O_3$ $[M + H]^+$). Anal. calcd for $C_{24}H_{19}FN_2O_3$: C, 71.63; H, 4.76; F, 4.72; N, 6.96; O, 11.93%. Found: C, 71.60; H, 4.79; F, 4.70; N, 6.97; O, 11.94%.

4.3.18. (3-(4-Methoxyphenyl)-1-phenyl-1*H*-pyrazol-4-yl) methyl 4-chlorobenzoate (10b). White powder, yield 85%, mp: 94–95 °C; ^{1}H NMR (300 MHz, $CDCl_3$) δ ppm: 3.80 (s, 3H); 5.40 (s, 2H); 7.00 (d, J = 5.22 Hz, 2H); 7.28 (t, J = 4.44 Hz, 1H); 7.41 (d, J = 5.13 Hz, 2H); 7.45 (t, J = 4.75 Hz, 2H); 7.74–7.77 (m, 4H); 7.98 (d, J = 5.22 Hz, 2H); 8.12 (s, 1H). ESI-MS: 419.87 ($C_{24}H_{20}ClN_2O_3$ $[M + H]^+$). Anal. calcd for $C_{24}H_{20}ClN_2O_3$: C, 68.82; H, 4.57; Cl, 8.46; N, 6.69; O, 11.46%. Found: C, 68.81; H, 4.58; Cl, 8.47; N, 6.68; O, 11.46%.

4.3.19. (3-(4-Methoxyphenyl)-1-phenyl-1*H*-pyrazol-4-yl) methyl benzoate (10c). White powder, yield 78%, mp: 107–109 °C; ^{1}H NMR (300 MHz, $CDCl_3$) δ ppm: 3.81 (s, 3H); 5.41 (s, 2H); 7.01 (d, J = 4.77 Hz, 2H); 7.28 (t, J = 4.44 Hz, 1H); 7.42–7.46 (m, 4H); 7.56 (t, J = 4.62 Hz, 1H); 7.72–7.79 (m, 4H); 8.06 (d, J = 4.95 Hz, 2H); 8.14 (s, 1H). ^{13}C NMR (100 MHz, $CDCl_3$) δ ppm: 166.61, 159.80, 152.48, 139.89, 133.17, 130.19, 129.70, 129.65, 129.47, 129.25, 128.51, 126.59, 125.28, 119.14, 115.39, 114.22, 57.91, 55.39. ESI-MS: 385.43 ($C_{24}H_{21}N_2O_3$ $[M + H]^+$). Anal. calcd for $C_{24}H_{21}N_2O_3$: C, 74.98; H, 5.24; N, 7.29; O, 12.49%. Found: C, 74.97; H, 5.23; N, 7.30; O, 12.50%.

4.3.20. (3-(4-Methoxyphenyl)-1-phenyl-1*H*-pyrazol-4-yl) methyl 4-methoxybenzoate (10d). White powder, yield 72%, mp: 100–103 °C; ^{1}H NMR (300 MHz, $CDCl_3$) δ ppm: 3.83 (s, 6H); 5.43 (s, 2H); 6.85 (d, J = 4.22 Hz, 2H); 7.02–7.10 (m, 4H); 7.45 (t, J = 4.22 Hz, 1H); 7.62 (t, J = 4.62 Hz, 4H); 7.91 (d, J = 5.14 Hz, 2H); 8.10 (s, 1H). ESI-MS: 415.45 ($C_{25}H_{23}N_2O_4$ $[M + H]^+$). Anal. calcd for $C_{25}H_{23}N_2O_4$: C, 72.42; H, 5.38; N, 6.71; O, 15.49%. Found: C, 72.44; H, 5.37; N, 6.71; O, 15.50%.

4.4. Crystal structure determination

Crystal structure determination of compound **9c** was carried out on a Nonius CAD4 diffractometer equipped with graphite-mono chromated MoKα (k = 0.71073 Å) radiation. The structure was solved by direct methods and refined on F^2 by full matrix least-squares methods using SHELX-97.[30] All non-hydrogen atoms of compound **9c** were refined with anisotropic thermal parameters. All hydrogen atoms were placed in geometrically idealized positions and constrained to ride on the parent atoms.

4.5. Antiproliferation assay

The antiproliferative activities of the prepared compounds against A375 and WM266.4 cells were evaluated as described elsewhere with some modifications.[31] Target tumor cell lines were grown to log phase in DMEM medium supplemented with 10% fetal bovine serum. After diluting to 2×10^4 cells per ml with the complete medium, 100 μL of the obtained cell suspension was added to each well of 96-well culture plates. The subsequent incubation was permitted at 37 °C, 5% CO_2 atmosphere for 24 h before the cytotoxicity assessments. Tested samples at pre-set concentrations were added to six wells with vemurafenib as positive references. After 48 h exposure period, 40 μL of PBS containing 0.5 mg ml^{-1} of MTT (3-(4,5-dimethylthiazol-2-yl)-2,5-diphenyltetrazolium bromide) was added to each well. After 4 h incubation, the optical absorbance was measured at 570 nm on an ELISA microplate reader. In all experiments three replicate wells were used for each drug concentration. Each assay was carried out for at least three times. The results were summarized in Table 1.

4.6. $BRAF^{V600E}$ enzymatic assay

7.5 ng Mouse Full-Length GST-tagged $BRAF^{V600E}$ (Invitrogen, PV3849) was preincubated at room temperature for 1 h with 1 μL drug and 4 μL assay dilution buffer. The kinase assay was initiated when 5 μL of a solution containing 200 ng recombinant human full length, N-terminal His-tagged MEK1 (Invitrogen, PV3093), 200 μM ATP (0.8 μCi hot ATP), and 30 mM $MgCl_2$ in assay dilution buffer was added. The kinase reaction was allowed to continue at room temperature for 25 min and was then quenched with 5 μL 5 × protein denaturing buffer

(LDS) solution. Protein was further denatured by heating for 5 min at 70 °C. 10 μL of each reaction was loaded into a 15 well, 4–12% precast NuPage gel (Invitrogen) and run at 200 V, and upon completion, the front, which contained excess hot ATP, was cut from the gel and discarded. The gel was then dried and developed onto a phosphor screen, which was scanned on a Storm 820 scanner and quantitated from optical densitometry using Image Quant v5.0. A reaction that contained no active enzyme was used as a negative control, and a reaction without inhibitor was used as the positive control. Final compound concentrations were 100 μM, 31.6 μM, 10 μM, 3.16 μM, 1 μM, 316 nM, 100 nM, 31.6 nM, 10 nM, 3.16 nM, 1 nM, 316 pM, and 100 pM.[32,33] The results were summarized in Table 2.

4.7. Kinase selectivity studies[34–36]

4.7.1. Serine/threonine kinase profiling by IC_{50} measurement. Assays for seven serine/threonine kinases using radio labeled [γ-^{32}P] ATP (GE Healthcare, Piscataway, NJ) were performed in 96 well plates. Mitogen-activated protein kinase p38α (p38α), was expressed as N-terminal FLAG-tagged protein using a baculovirus expression system. Aurora-A and -B were expressed as N-terminal 6xHis tagged protein using a baculovirus expression system. MEK1 was expressed as N-terminal GST fusion protein using a freestyle 293 expression system. Cyclin-dependent kinase 1 (CDK1)/CycB and CDK2/CycA were expressed as C-terminal 6His-tagged CDK2, and N-terminal GST-tagged Cyclin A protein using a baculovirus expression system.

The reaction conditions were optimized for each kinase: p38α (100 ng per well of enzyme, 1 μg per well of MBP (Wako Pure Chemical Ind., Osaka, Japan), 0.1 μCi per well of [γ-^{32}P] ATP, 60 min reaction at 30 °C); BRF^{V600E} (25 ng per well of enzyme, 1 μg per well of GST-MEK1(K96R), 0.1 μCi per well of [γ-^{33}P] ATP, 20 min reaction at room temperature); Aurora-A and -B (50 ng per well of enzyme, 30 μM of Aurora substrate peptide, 0.2 μCi per well of [γ-^{32}P] ATP, 60 min reaction at room temperature); MEK1 (100 ng per well of enzyme, 0.3 μg per well of GST-ERK1 (K71A) 0.2 μCi per well of [γ-^{33}P] ATP, 20 min reaction at room temperature); CDK1/CycB (4.2 ng per well of enzyme, 1 μg per well of Histone H1 (Calbiochem), 0.2 μCi/well of [γ-^{33}P] ATP, 20 min reaction at room temperature); CDK2/CycA (1.8 mUnits per well of enzyme, 1 μg per well of Histone H1 (Calbiochem), 0.2 μCi per well of [γ-^{32}P] ATP, 20 min reaction at room temperature).

All the seven enzyme reactions were performed in 25 mM HEPES, pH 7.5, 10 mM magnesium acetate, 1 mM dithiothreitol and 0.5 μM ATP containing optimized concentration of enzyme, substrate and radio labeled ATP as described above in a total volume of 50 μl. Prior to the kinase reaction, compound and enzyme were incubated for 5 min at reaction temperature as described above. The kinase reactions were initiated by adding ATP. After the reaction period as described above, the reactions were terminated by the addition of 10% (final concentration) trichloroacetic acid. The [γ-^{32}P]-phosphorylated proteins were filtrated in Harvest Plate (Millipore Corp.) with a Cell Harvester (PerkinElmer) and then free of [γ-^{32}P] ATP was washed out with 3% phosphoric acid. The plates were dried, followed by the addition of 40 μl of MicroScint0 (PerkinElmer). The radioactivity was counted by a Top Count scintillation counter (PerkinElmer). The results were summarized in Table 3.

4.7.2. Tyrosine kinase profiling by IC_{50} measurement. The cytoplasmic domain of vascular endothelial growth factor receptor 2 (VEGFR2), platelet-derived growth factor receptor α (PDGFRα) and cSRC were purchased from Millipore Corp. Assays for 3 tyrosine kinases were performed in 384 well plates using the Alphascreen® system (PerkinElmer) at room temperature. Enzyme reactions were performed in 50 mM Tris–HCl, pH 7.5, 5 mM $MnCl_2$, 5 mM $MgCl_2$, 0.01% Tween-20, 2 mM dithiothreitol and 0.1 μg ml^{-1} biotinylated poly-GluTyr (4 : 1) containing optimized concentration of enzyme and ATP as described below.

Prior to the kinase reaction, compound and enzyme were incubated for 5 min at room temperature. The reactions were initiated by adding ATP. After the reaction period as described below at room temperature, the reactions were stopped by the addition of 25 μl of 100 mM EDTA, 10 μg ml^{-1} Alphascreen streptavidin donor beads and 10 μg ml^{-1} acceptor beads described below in 62.5 mM HEPES, pH 7.4, 250 mM NaCl, and 0.1% BSA. Plates were incubated in the dark for more than 12 h and then read by EnVision 2102 Multilabel Reader (PerkinElmer). The well containing substrate and enzyme without compound was used as total reaction control. The reaction conditions for these 10 kinases were optimized for each kinase: VEGFR2 (19 ng ml^{-1} of enzyme, 10 μM ATP, 10 min reaction, PY-100 conjugated acceptor beads (PY-100)); PDGFRα (50 ng ml^{-1} of enzyme, 10 μM ATP, 30 min reaction, PT66 conjugated acceptor beads (PT66)); cSrc (0.33 ng ml^{-1} of enzyme, 2 μM ATP, 10 min reaction, PY-100). The results were summarized in Table 3.

4.8. Molecular docking study

Molecular docking of compounds into the 3D BRAF^{V600E} complex structure (PDB code: 2FB8) was carried out using the Discovery Studio (version 3.5) as implemented through the graphical user interface CDOCKER protocol. The three-dimensional structures of the aforementioned compounds were constructed using Chem 3D ultra 11.0 software [Chemical Structure Drawing Standard; Cambridge Soft corporation, USA (2010)], then they were energetically minimized by using MOPAC with 5000 iterations and minimum RMS gradient of 0.10. The crystal structures of BRAF complex were retrieved from the RCSB Protein Data Bank (http://www.rcsb.org/pdb/home/home.-do). All bound water and ligands were eliminated from the protein and the polar hydrogen was added. The whole BRAF^{V600E} complex was defined as a receptor and the site sphere was selected based on the ligand binding location.

4.9. 3D-QSAR

Ligand-based 3D-QSAR approach was performed by QSAR software of the DS 3.5 (Discovery Studio 3.5, Accelrys, Co. Ltd). The training sets were composed of 16 inhibitors with the corresponding pIC_{50} values which were converted from the obtained IC_{50} (μM), and test sets comprised 4 compounds. All

the definition of the descriptors can be seen in the help of DS 3.5 software and they were calculated by QSAR protocol of DS 3.5. The alignment conformation of each molecule was the one with lowest interaction energy in the docked results of CDOCKER (generated in molecular CDOCKER). The predictive ability of 3D-QSAR modeling can be evaluated based on the cross-validated correlation coefficient, which qualifies the predictive ability of the models. Scrambled test (Y scrambling) was performed to investigate the risk of chance correlations. The inhibitory potencies of compounds were randomly reordered for 30 times and subject to leave-one-out validation test, respectively. The models were also validated by test sets, in which the compounds are not included in the training sets. Usually, one can believe that the modeling is reliable, when the r^2 for test sets is larger than 0.6, respectively.

Acknowledgements

This work was supported by the open foundation from State Key Laboratory of Pollution Control and Resource Reuse, Nanjing University, Nanjing 210093, PR China.

References and notes

1 M. J. Robinson and M. H. Cobb, *Curr. Opin. Cell Biol.*, 1997, **9**, 180–186.
2 S. Ramurthy, S. Subramanian, M. Aikawa, P. Amiri, A. Costales, J. Dove, S. Fong, J. M. Jansen, B. Levine, S. Ma, C. M. Mcbride, J. Michaelian, T. Pick, D. J. Poon, S. Girish, C. M. Shafer, D. Stuart, L. Sung and P. A. Renhowe, *J. Med. Chem.*, 2008, **51**, 7049–7052.
3 P. J. Roberts and C. J. Der, *Oncogene*, 2007, **26**, 3291–3310.
4 M. J. Garnett and R. Marais, *Cancer Cell*, 2004, **6**, 313–319.
5 N. Ishimura, K. Yamasawa, R. M. Karim, Y. Kadowaki, S. Ishihara, Y. Amano, Y. Nio, T. Higami and Y. Kinoshita, *Cancer Lett.*, 2003, **199**, 169–173.
6 N. Li, D. Batt and M. Warmuth, *Curr. Opin. Invest. Drugs*, 2007, **8**, 452–456.
7 D. A. Tuveson, B. L. Weber and M. Herlyn, *Cancer Cell*, 2003, **4**, 95–98.
8 R. Kumar, S. Angelini, K. Czene, I. Sauroja, M. Hahka-Kemppinen, S. Pyrhonen and K. Hemminki, *Clin. Cancer Res.*, 2003, **9**, 3362–3368.
9 T. Fukushima, S. Suzuki, M. Mashiko, T. Ohtake, Y. Endo, Y. Takebayashi, K. Sekikawa, K. Hagiwara and S. Takenoshita, *Oncogene*, 2003, **22**, 6455–6457.
10 H. Davies, G. R. Bignell, C. Cox, P. Stephens, S. Edkins, S. Clegg, J. Teague, H. Woffendin, M. J. Garnett, W. Bottomley, N. Davis, E. Dicks, R. Ewing, Y. Floyd, K. Gray, S. Hall, R. Hawes, J. Hughes, V. Kosmidou, A. Menzies, C. Mould, A. Parker, C. Stevens, S. Watt, S. Hooper, R. Wilson, H. Jayatilake, B. A. Gusterson, C. Cooper, J. Shipley, D. Hargrave, K. Pritchard-Jones, N. Maitland, G. Chenevix-Trench, G. J. Riggins, D. D. Bigner, G. Palmieri, A. Cossu, A. Flanagan, A. Nicholson, J. W. Ho, S. Y. Leung, S. T. Yuen, B. L. Weber, H. F. Seigler, T. L. Darrow, H. Paterson, R. Marais, C. J. Marshall, R. Wooster, M. R. Stratton and P. A. Futreal, *Nature*, 2002, **417**, 949–954.
11 M. Karasarides, A. Chiloeches, R. Hayward, D. Niculescu-Duvaz, I. Scanlon, F. Friedlos, L. Ogilvie, D. Hedley, J. Martin, C. J. Marshall, C. J. Springer and R. Marais, *Oncogene*, 2004, **23**, 6292–6298.
12 S. R. Hingorani, M. A. Jacobetz, G. P. Robertson, M. Herlyn and D. A. Tuveson, *Cancer Res.*, 2003, **63**, 5198–5202.
13 R. Ng and E. X. Chen, *Curr. Clin. Pharmacol.*, 2006, **1**, 223–228.
14 T. Eisen, T. Ahmad and T. K. Flaherty, *Br. J. Cancer*, 2006, **95**, 581–586.
15 S. M. Wilhelm, C. Carter, L. Tang, D. Wilkie, A. Mcnabola, H. Rong, C. Chen, X. Zhang, P. Vincent, M. Mchugh, Y. Cao, J. Shujath, S. Gawlak, D. Eveleigh, B. Rowley, L. Liu, L. Adnane, M. Lynch, D. Auclair, I. Taylor, R. Gedrich, A. Voznesensky, B. Riedl, L. E. Post, G. Bollag and P. A. Trail, *Cancer Res.*, 2004, **64**, 7099–7109.
16 I. Niculescu-Duvaz, E. Roman, S. R. Whittaker, F. Friedlos, R. Kirk, I. J. Scanlon, L. C. Davies, D. Niculescu-Duvaz, R. Marais and C. J. Springer, *J. Med. Chem.*, 2006, **49**, 407–416.
17 T. Ahmad and T. Eisen, *Clin. Cancer Res.*, 2004, **10**, 6388S–6392S.
18 D. Niculescu-Duvaz, C. Gaulon, H. P. Dijkstra, I. Niculescu-Duvaz, A. Zambon, D. Menard, B. M. Suijkerbuijk, A. Nourry, L. Davies, H. Manne, F. Friedlos, L. Ogilvie, D. Hedley, S. Whittaker, R. Kirk, A. Gill, R. D. Taylor, F. I. Raynaud, J. Moreno-Farre, R. Marais and C. J. Springer, *J. Med. Chem.*, 2009, **52**, 2255–2264.
19 I. Niculescu-Duvaz, E. Roman, S. R. Whittaker, F. Friedlos, R. Kirk, I. J. Scanlon, L. C. Davies, D. Niculescu-Duvaz, R. Marais and C. J. Springer, *J. Med. Chem.*, 2008, **51**, 3261–3274.
20 C. Luo, P. Xie and R. Marmorstein, *J. Med. Chem.*, 2008, **51**, 6121–6127.
21 K. T. Flaherty, I. Puzanov, K. B. Kim, A. Ribas, G. A. Mcarthur, J. A. Sosman, P. J. O'Dwyer, R. J. Lee, J. F. Grippo, K. Nolop and P. B. Chapman, *N. Engl. J. Med.*, 2010, **363**, 809–819.
22 G. K. Schwartz, S. Robertson, A. Shen, E. Wang, L. Pace, H. Dials, D. Mendelson, P. Shannon and M. Gordon, *J. Clin. Oncol.*, 2009, **27**, 3513.
23 D. C. Heimbrook, H. E. Huber, S. M. Stirdivant, D. R. Patrick, D. Claremon, N. Liverton, H. Selnick, J. Ahern, R. Conroy, R. Drakas, N. Falconi, P. Hancock, R. Robinson, G. Smith and A. Olif, *89th Meeting of the American Association for Cancer Research*, New Orleans, Mar 28–Apr 1, 1998, vol. 24, p. 3793.
24 A. J. King, D. R. Patrick, R. S. Batorsky, M. L. Ho, H. T. Do, S. Y. Zhang, R. Kumar, D. W. Rusnak, A. K. Takle, D. M. Wilson, E. Hugger, L. Wang, F. Karreth, J. C. Lougheed, J. Lee, D. Chau, T. J. Stout, E. W. May, C. M. Rominger, M. D. Schaber, L. Luo, A. S. Lakdawala, J. L. Adams, R. G. Contractor, K. S. Smalley, M. Herlyn, M. M. Morrissey, D. A. Tuveson and P. S. Huang, *Cancer Res.*, 2006, **66**, 11100–11105.

25 Q. S. Li, C. Y. Li, X. Lu, H. Zhang and H. L. Zhu, *Eur. J. Med. Chem.*, 2012, **50**, 288–295.
26 Q. S. Li, X. H. Lv, Y. B. Zhang, J. J. Dong, W. P. Zhou, Y. Yang and H. L. Zhu, *Bioorg. Med. Chem. Lett.*, 2012, **22**, 6596–6601.
27 X. Li, X. Lu, M. Xing, X. H. Yang, T. T. Zhao, H. B. Gong and H. L. Zhu, *Bioorg. Med. Chem. Lett.*, 2012, **22**, 3589–3593.
28 X. F. Huang, X. Lu, Y. Zhang, G. Q. Song, Q. L. He, Q. S. Li, X. H. Yang, Y. Wei and H. L. Zhu, *Bioorg. Med. Chem.*, 2012, **20**, 4895–4900.
29 X. Li, J. L. Liu, X. H. Yang, X. Lu, T. T. Zhao, H. B. Gong and H. L. Zhu, *Bioorg. Med. Chem.*, 2012, **20**, 4430–4436.
30 G. M. Sheldrick, *SHELX-97. Program for X-ray Crystal Structure Solution and Refinement*, Göttingen University, Germany, 1997.
31 A. Boumendjel, J. Boccard, P. A. Carrupt, E. Nicolle, M. Blanc, A. Geze, L. Choisnard, D. Wouessidjewe, E. L. Matera and C. Dumontet, *J. Med. Chem.*, 2008, **51**, 2307–2310.
32 J. Dietrich, V. Gokhale, X. Wang, L. H. Hurley and G. A. Flynn, *Bioorg. Med. Chem.*, 2010, **18**, 292–304.
33 I. Niculescu-Duvaz, E. Roman, S. R. Whittaker, F. Friedlos, R. Kirk, I. J. Scanlon, L. C. Davies, D. Niculescu-Duvaz, R. Marais and C. J. Springer, *J. Med. Chem.*, 2006, **49**, 407–416.
34 M. Saitoh, J. Kunitomo, E. Kimura, Y. Hayase, H. Kobayashi, N. Uchiyama, T. Kawamoto, T. Tanaka, C. D. Mol, D. R. Dougan, G. S. Textor, G. P. Snell and F. Itoh, *Bioorg. Med. Chem.*, 2009, **17**, 2017–2029.
35 C. Hundsdorfer, H. J. Hemmerling, J. Hamberger, M. Le Borgne, P. Bednarski, C. Gotz, F. Totzke and J. Jose, *Biochem. Biophys. Res. Commun.*, 2012, **424**, 71–75.
36 D. D. Li, Y. J. Qin, J. Sun, J. R. Li, F. Fang, Q. R. Du, Y. Qqian, H. B. Gong and H. L. Zhu, *PLoS One*, 2013, **8**, 1–11.